Multiphase autoresonant excitations in discrete nonlinear Schrödinger systems

Y. Gopher and L. Friedland
Racah Institute of Physics, Hebrew University of Jerusalem, Jerusalem 91904, Israel

A. G. Shagalov
Institute of Metal Physics, Ekaterinburg 620219, Russian Federation
(Received 13 May 2005; published 12 September 2005)

Large amplitude, multiphase solutions of periodic discrete nonlinear Schrödinger (NLS) systems are excited and controlled by starting from zero and using a small perturbation. The approach involves successive formation of phases in the solution by driving the system with small amplitude plane wavelike perturbations (drives) with chirped frequencies, slowly passing through a system's resonant frequency. The system is captured into resonance and enters a continuing phase-locking (autoresonance) stage, if the drive's amplitude surpasses a certain sharp threshold value. This phase-locked solution is efficiently controlled by variation of an external parameter (driving frequency). Numerical examples of excitation of multiphase waves and periodic discrete breathers by using this approach for integrable (Ablowitz-Ladik) and nonintegrable NLS discretizations are presented. The excited multiphase waveforms are analyzed via the spectral theory of the inverse scattering method applied to both the integrable and nonintegrable systems. A theory of autoresonant excitation of 0- and 1-phase solutions by passage through resonances is developed. The threshold phenomenon in these cases is analyzed.

DOI: 10.1103/PhysRevE.72.036604 PACS number(s): 05.45.Yv, 05.45.Xt, 89.75.Kd

I. INTRODUCTION

The nonlinear Schrödinger (NLS) equation

$$i\psi_t = \psi_{xx} + 2\sigma|\psi|^2\psi, \quad \sigma = \pm 1, \tag{1}$$

where $\psi=\psi(x,t)$ is one of the most important equations of nonlinear physics and describes a wide variety of physical phenomena, ranging from light pulse propagation in optical fibers, through nonlinear modulations of plasma waves to Bose-Einstein condensations [1]. Its discrete forms (DNLS),

$$i\frac{dq_n}{dt} = \frac{1}{\Delta^2}(q_{n+1} + q_{n-1} - 2q_n) + N_n, \tag{2}$$

where $q_n=q_n(t)$, $N_n=\sigma|q_n|^2[(1-\nu)(q_{n+1}+q_{n-1})+2\nu q_n]$, and $0\leqslant\nu\leqslant 1$ also draw much attention both as mere discretizations of the continuous NLS (used in numerical simulations) and also independently, as models for discrete lattices. There is a growing interest in these lattices due to their relevance in various fields of physics. One such field is nonlinear optics, where DNLS models coupled waveguide arrays. Initially proposed by Christodulides and Joseph [2] there are many studies of the properties of waveguide arrays, with the goal of designing optical switching devices and, ultimately, of all-optical signal processing devices [3–5]. In biophysics DNLS was studied by Davydov [6] describing the propagation of excitations in molecular chains. In solid-state physics it describes the dynamics of Bose-Einstein condensates in an optical lattice [7,8]. There are also many further applications in undriven [1,9,10] and driven [11,12] DNLS systems. The present work is devoted to the study of the periodic, $q_{n+M}(t)=q_n(t)$, most common discretizations, which are those with $\nu=0,1$ and are known as the integrable discrete NLS (IDNLS):

$$i\frac{dq_n}{dt} = \frac{1}{\Delta^2}(q_{n+1} + q_{n-1} - 2q_n) + \sigma|q_n|^2(q_{n+1} + q_{n-1}) \tag{3}$$

and the diagonal discrete NLS (DDNLS),

$$i\frac{dq_n}{dt} = \frac{1}{\Delta^2}(q_{n+1} + q_{n-1} - 2q_n) + 2\sigma|q_n|^2 q_n, \tag{4}$$

respectively. These two discretizations seem alike, since they are both Hamiltonian and tend to (1) as $\Delta\to 0$, $M\to\infty$ and $M\Delta\to$ const. Yet they are profoundly different; while IDNLS is integrable, DDNLS is not and may exhibit chaotic behavior [13]. Nevertheless, it is the DDNLS equation, which has a large number of important physical applications.

The most general tool of analysis available for IDNLS (3) is the inverse scattering transform (IST) which is a method of solving certain classes of nonlinear differential equations. First introduced by Gardner *et al.* in 1967 [14] as a method for solving the Korteweg–de Vries (KdV) equation, it was later generalized to include many different nonlinear evolution equations. In 1972 Zhakharov and Shabat extended the method to NLS [15], and further on Ablowitz and Ladik extended it to discrete systems including IDNLS Eq. (3) (also known as Ablowitz-Ladik model) [16,17]. For details on the application of IST to IDNLS see Ref. [1]. Using IST analysis we learn a great deal on the types and structure of the multitude of solutions admitted by (3), among such solutions are the plane wave solution ($q_n=ae^{i(\kappa n-\omega t)}; \forall n$), solitons [1], and discrete breathers (DB), or rather intrinsic localized modes [18]. The most general solution admitted by periodic IDNLS Eq. (3) is a nontrivial function of many phases [19], i.e., of the form $q_n=f(\Theta_0,\Theta_1,\ldots)$, where Θ_i are phase variables of form $\Theta_i=\kappa_i n-\omega_i t$, κ_i,ω_i are constant, and n is the lattice site number. For example, periodic IDNLS

breathers are characterized by three phases (see Sec. II C below). The practical realization of these multiphase IDNLS solutions is not easily accomplished since it requires calculating and realizing specific initial conditions, neither of which is always feasible.

Our goal in this paper is to propose a simple scheme which allows excitations of muiltiphase solutions from zero initial conditions ($q_n=0\ \forall n$). This goal will be achieved by replacing (3) with a perturbed problem,

$$i\frac{dq_n}{dt}=\frac{1}{\Delta^2}(q_{n+1}+q_{n-1}-2q_n)+\sigma|q_n|^2(q_{n+1}+q_{n-1})+f(n,t), \tag{5}$$

where $|f(n,t)|\ll 1$ and we propose a simple drive function $f(n,t)$ which will excite and control the aforementioned multiphase solutions. The spectral theory of the IST method for IDNLS will be used as the main diagnostic tool for characterizing the excited waveforms. A similar scheme for continuous NLS systems has recently been studied in Ref. [20]. As for DDNLS (4), being nonintegrable, we do not have an analytical tool such as IST, so we shall apply a more numerical approach. We shall still use the same excitation recipe and examine the range of its validity numerically by testing the number of phases in the excited solution directly in the simplest, one- and two-phase excitations. In more complex situations, we shall continue multiphase DDNLS solutions numerically to those of the IDNLS equation, where one can apply the IST approach for diagnostics. Thus, we shall develop an indirect IST diagnostics for studying multiphase solutions of important in applications, but nonintegrable, DDNLS equation.

Our excitation and control scheme is based on the concept of autoresonance. Autoresonance is a phenomenon of nonlinear physics in which a driven nonlinear system remains phase locked to a driving oscillation despite adiabatic variations of the drive's frequency. The autoresonance idea originated 60 years ago in applications to relativistic particle accelerators [21–23]. Much later similar ideas were applied to other dynamical [24–31] and extended [32–42] systems. For exciting multiphase waves, we proceed in stages from a $(m-1)$-phase solution, drive the system with a simple drive function $f(n,t)$ (a plane wave) with a specific frequency and slowly change (chirp) that frequency, passing through the system's resonance with a new, mth frequency. The objective is to resonantly form and control the desired m phase in the system. We shall show that under certain conditions, the passage through the resonance yields an efficient capture into resonance followed by a persistent adiabatic phase locking between the new, mth, phase and the drive despite variation of the driving frequency. In this terminology, the driven system is said to be in autoresonance. In this state, the newly formed mth wave frequency self-adjusts to that of the drive and, as the result, the perturbed systems travel through the space of m-phase solutions of the unperturbed system. Then, at a desired time, one replaces the driving term by a similar one, but with a different frequency and frequency chirp, trying to autoresonantly form another $(m+1)$st phase in the solution and so on. Such successive autoresonant excitation allows us to form the desired number of phases in the solution, by starting from zero, as well as control the solution by autoresonance at each excitation stage. A similar approach was recently applied to several other integrable systems possessing multiphase solutions, such as the Korteweg–de Vries (KdV) equation [43], Toda lattice [31], and NLS equation [20]. Here, we focus on excitation and control of multiphase solutions of both integrable and nonintegrable periodic DNLS systems.

The paper is organized as follows: In Sec. II we present our excitation scheme in numerical simulations. We shall demonstrate emergence of 0-phase solutions [plane waves, $q_n=a\exp(i\Theta_0)$, see below], as well as, one-, two-, and three-phase waves for the integrable and nonintegrable cases. We shall encounter and numerically illustrate the threshold for synchronization, which is a universal phenomenon of many driven nonlinear systems [30,39] that dictates a minimum drive's amplitude for capturing the system in autoresonance by passage through resonances. In Sec. III we shall present a theoretical analysis of the 0-phase autoresonant excitation and study stability of that solution. In the same section we shall analyze the corresponding threshold phenomenon. Section IV will describe the theory of excitation of 1-phase solutions according to our scheme, i.e., by successively exciting a 0-phase solution and then a 1-phase solution, and considering the threshold phenomenon in the second excitation stage. In Sec. V we shall discuss excitation of multiphase solutions of the DDNLS equation in more detail, its chaotic behavior, and give a numerical criterion for the evasion thereof. In the same section, we shall analyze multiphase solutions of DDNLS by continuation to the associated IDNLS problem allowing the IST diagnostics. Finally, Sec. VI will present our conclusions.

II. MULTIPHASE EXCITATIONS IN NUMERICAL SIMULATIONS

In this section we present results of numerical simulations demonstrating our approach to excitation and control of multiphase solutions in discrete, periodic ($q_{i+M}=q_i$) NLS systems.

A. Driven multiphase IDNLS waves

We shall proceed from an example for periodic IDNLS equation (3). Multiphase periodic IDNLS solutions have the form (see Appendix A)

$$q_n(t)=W(\Theta_1,\ldots,\Theta_m)e^{i\Theta_0}, \tag{6}$$

where $W=W(\Theta)$ is a complex function of m phases $\Theta_i=\kappa_i n-\omega_i t$, $i=1,\ldots,m$, $m<M$ (internal phases), $\Theta_0=\kappa_0 n-\omega_0 t$ referred to as the external phase, and the wave numbers κ_i and frequencies ω_i are constants. Because of periodicity, $\kappa_i=m_i\kappa_0$, where $\{m_i\}$ is a set of different integers, $0\leqslant m_i<M$, and $\kappa_0=2\pi/M$.

Our example focuses on the case of periodicity $M=5$, and $\Delta=0.6$ (here and in the following, without loss of generality, we use dimensionless dependent and independent variables and parameters). The goal is to excite a 3-phase solution of

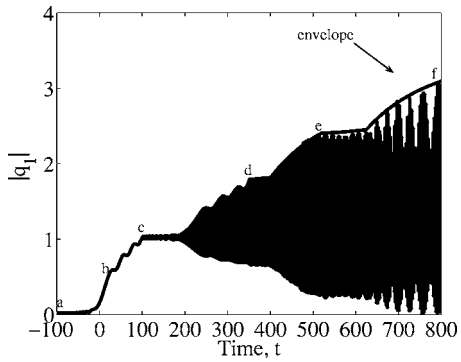

FIG. 1. Time evolution of $|q_1|$. The letters indicate significant time stamps, (a) start of application of the first plane wave drive, (b) intermediate point of autoresonant excitation of a flat solution, (c)–(f) ends of application of the first, second, third, and fourth drives. A developed three-phase solution is formed at point (f).

form (6) with $m=3$. We proceed by numerically solving the perturbed problem (5) with initial conditions $q_i=0$ and set the drive function f to be a plane wave $f_0=\varepsilon_0 \exp\{i[m_0\kappa_0 - \int \omega_{d0}(t)dt]\}$, where $m_0=0$, the frequency is chirped according to $\omega_{d0}(t)=\omega_{r0}+\alpha_0 t$, α_0 is a constant chirp rate (where we set sign $\alpha=\sigma$) and ω_{r0} is a constant, such that at $t=0$, ω_{d0} is in resonance with one of the linear frequencies of the unperturbed system ($\omega_{r0}=0$, in this example). At $t>0$ a slightly perturbed plane wave of growing amplitude will be excited. In autoresonance, the frequency of this plane wave is phase locked with that of the drive $\omega_0(t)\approx\omega_{d0}(t)$. A general discussion of this stage of excitation will be given in Sec. III. At a given time $t=t_1$, we proceed by exciting another phase, this is done by turning f_0 off and applying a drive, $f_1 = \varepsilon_1 \exp\{i[m_1\kappa_0 - \int \omega_{d1}(t)dt]\}$, when this time $m_1=1$, $\omega_{d1}(t) = \omega_{r1}+\alpha_1 t$, $\omega_{r1}\neq 0$. A correct choice of ω_{r1} will ensure that at a given time, say t_{r1} the drive's frequency will slowly pass through the resonance frequency associated with the sum of the external phase and that having $\kappa_1=\kappa_0$ ($m_1=1$), meaning $\omega_{d1}(t_{r1})=\omega_0(t_{r1})+\omega_1(t_{r1})$. This passage through resonance excites the desired phase and the solution becomes a slightly perturbed 1-phase solution. The system is again trapped in resonance with the drive, so as long as the drive is applied the amplitude of the 1-phase solution will grow and the excited phase's frequency will be locked with the drive's frequency ($\omega_{d1}\approx\omega_0+\omega_1$), and, therefore, is completely controlled by the drive. We shall analyze this stage of excitation in more detail in Sec. IV. Next, we proceed to excite two more phases, at time $t=t_2$, f_1 is turned off and a new chirped frequency drive f_2 with $m_2=2$ is applied, passing and trapping another phase in resonance at $t=t_{r2}$, and so on for the $m_3=3$ mode. At the end of the process we have a solution with exactly three phases. The whole excitation procedure in our example is illustrated in Fig. 1 presenting the evolution of $|q_1|$ and its envelope. For this simulation we used $\alpha_i = [0.02, 0.01, 0.01, 0.005]$, $\varepsilon_i = [0.02, 0.06, 0.005, 0.03]$, $\omega_{ri} = [0, 11.64, 0.455, 13.10]$, and the drives were changed at times $t_i=[-100, 100, 350, 520]$. The letters (a), (c), (d), (e), and (f) in Fig. 1 mark the beginnings and ends of time windows where a particular drive has been present in simulations. In addition, the actual waveform in a small time window $t\in[600,610]$ is illustrated in Fig. 2, showing $\mathrm{Re}(q_n)$ after the excitation of two internal phases, where we applied the same drive as before but stopped the drive completely at $t=520$ and allowed an unperturbed IDNLS solution evolve. Note that the solution seems highly irregular, but through IST analysis we know that it is composed of exactly three phases (two internal and one external), see Fig. 4(e) below.

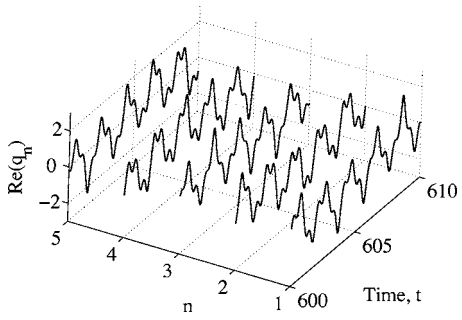

FIG. 2. Evolution of $\mathrm{Re}(q_n)$ in a two phase (plus 1 external phase) solution in a time window $t\in[600,610]$.

An important phenomenon encountered in our simulations was that of the aforementioned synchronization threshold. One finds at each excitation stage that there is a sharp threshold value for ε_i beneath which autoresonance does not occur (the system is excited slightly via passage through resonance, but, as the amplitude grows, it falls out of resonance with the drive) and above which autoresonance does occur. This effect is demonstrated in Fig. 3. Shown is the upper envelopes of $|q_1|$ as a function of time for five similar simulations, one (the solid line) is the same as shown in Figs. 1 and 4 others are the same but in each one, at a different excitation stage, we set the driving amplitude to a value lower by a few percent than the threshold, $\varepsilon_i^{\mathrm{th}}=[0.016, 0.055, 0.006, 0.03]$. One can see in Fig. 3 that below the threshold the amplitude's growth is stopped at the stage where the drive amplitude is not large enough.

Up to this point two statements still need to be proven. First, that the number of excited phases at each stage in Fig. 1 is *exactly* 0 (a plane wave), 1, 2, and 3. Second, that the system is phased locked, i.e., at every excitation stage

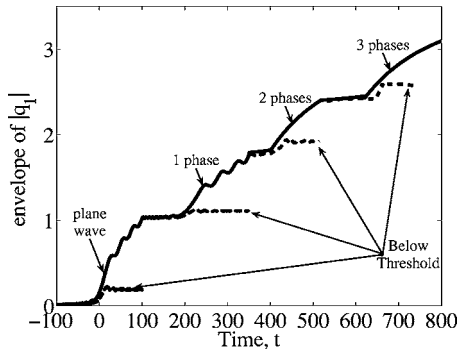

FIG. 3. Threshold phenomenon. The thick solid line shows the envelope of a solution with all drives above the thresholds for synchronization, the dashed lines are envelopes of solutions where at different stages of excitation the drive amplitude is slightly below the threshold value and the system falls out of resonance.

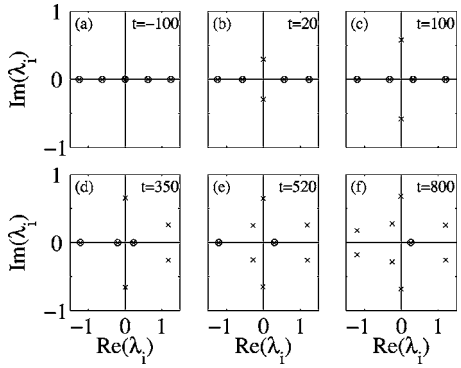

FIG. 4. The main spectrum at different times. The letters correspond with the notation in Fig. 1, namely at the beginning (a) through the evolution of the 0th phase (b), (c) in which the initially degenerate pair is constantly further excited and the gap between them grows, at the end of the excitation of the first (d), second (e), and third (f) phases. In the end there are three nondegenerate complex conjugated pairs, and one degenerate pair, or rather unexcited phase.

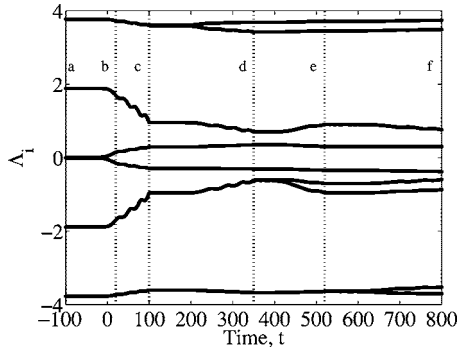

FIG. 5. An alternative representation of the main spectrum's time evolution. Shown is the quantity $\Lambda_i=3\,\mathrm{Re}(\lambda_i)+0.5\,\mathrm{Im}(\Lambda_i)$ as a function of time. The average of any open pair of spectral points is 3 times the real value of that pair and the size of the gap between them is the (absolute value of the) imaginary part of the pair. The dashed lines and letters correspond the notations in Figs. 1 and 4.

i, $\omega_{di}(t)\approx\omega_0(t)+\omega_i(t)$. For testing both these statements, we use the spectral IST analysis (see Ref. [19] and Appendix A for details). The IST theory shows that an unperturbed periodic IDNLS lattice with M sites has $2M$ conserved quantities, denoted λ_i (for definition, see Appendix A) and referred to as the main spectrum in the following. In the case of the focusing IDNLS, the main spectrum λ_j comprises M pairs of complex conjugated parameters $\lambda_i^{(1)}=\lambda_i^{(2)*}$, $i=1,\ldots,M$. In the defocusing case all λ_j are real. A degenerate pair of spectral values indicates an unexcited degree of freedom (phase) and a nondegenerate pair of complex conjugated spectral points (in the focusing case), denoted $\lambda_j^{(1)}=\lambda_j^{(2)*}$ represents an excited phase. If the driving perturbation is small, the system is close to some solution of the unperturbed system (dual solution in the following) at any given time t. For example, one can use the solution of the perturbed system at time t as initial data for generating a dual solution of the unperturbed system. By analyzing the main spectrum of this unperturbed solution one can examine how many of the possible phases in the perturbed problem are excited and how many are dormant at time t. This diagnostics is demonstrated in Fig. 4 showing a snapshot evolution of the spectrum in time. The times of the snapshots are shown in the figure together with letters (a),(b),…,(f) at each time corresponding to the same letters in Fig. 1. We begin [Fig. 4(a)] from a zero solution ($q=0$), whereby all spectral points pairs are degenerate. As the 0th phase solution is excited [see Fig. 4(b)] the degeneracy of one pair is removed. As long as the drive is applied, and hence the plane wave amplitude grows, the distance (or gap) between the pair grows [Fig. 4(b)]. As further phases are excited, other gaps are opened [Figs. 4(c)–4(f)].

An alternative way of presenting the main spectrum's time evolution is to show the quantity $\Lambda_i=C\,\mathrm{Re}(\lambda_i)+\frac{1}{2}\,\mathrm{Im}(\lambda_i)$ where C is some constant (chosen for presentability reasons) as a function of time. Remembering that the spectrum is comprised of complex conjugate pairs, we can deduce that the average (denoted a) of any pair of Λ's (say $\Lambda_{1,2}$) is simply C times the real value of both λ_1 and λ_2, and the gap between them (say d) is simply the imaginary part of one of the pair (i.e. $\lambda_1=a/C+id$, $\lambda_2=a/C-id$). This is a roundabout way of showing the spectrum, but it allows to show the entire time evolution of the spectrum. Figure 5 represents the main spectrum of the example in Fig. 1 in this way with $C=3$ to avoid line intersections. The vertical dotted lines denoted by letters (a)–(f) in the figure indicate the time moments corresponding to the same letters in Figs. 1 and 4. One can clearly see the openings of four different gaps in the spectrum due to passage through resonances, indicating successive formation of the external phase and three additional (internal) phases in the excited solution.

Given the main spectrum, using the IST theory (see Appendix A), we can calculate the internal frequencies $\omega_1\cdots\omega_{M-1}$ at any given time. However, for the external frequency ω_0 we must deploy a different numerical strategy. Every given time interval we stopped the simulation and used the result at that time, say $q_n(t^*)$ as the initial conditions of an unperturbed IDNLS system and ran such a simulation for a long time period $T\gg\max\{2\pi/\omega_j\}$. For finding ω_0, we defined the average, $Q(t)=\Sigma_{n=1}^{M}q_n(t)$, and wrote it as $Q(t)=U\exp[i(\xi+V)]$, where both U and V are real and quasiperiodic in time. Then, we calculated $d(\ln Q)/dt=d(\ln U)/dt+i(dV/dt-\omega_0)$, yielding $\mathrm{Im}[d(\ln Q)/dt]=dV/dt-\omega_0$. Since the long time average of dV/dt vanishes, the averaging of $\mathrm{Im}[d(\ln Q)/dt]$ over T yielded the desired value of ω_0 at any given t^*. Armed with methods to calculate all frequencies in the solution, we could ascertain that the system was truly phase locked at each stage. This test is presented in Fig. 6 showing the computed value of $\omega_0(t)$ and the set $\omega_0(t)+\omega_i(t)$ for the example shown in Fig. 1. The straight segments in the figure show the driving frequencies in the corresponding time intervals. We see how different system's frequencies adjust themselves to the drive frequencies at each stage of excitation and, consequently, the corresponding different phases are locked to the drive.

B. Multiphase DDNLS waves

In this example we use our excitation procedure to form multiphase periodic DDNLS waves. The solutions of this

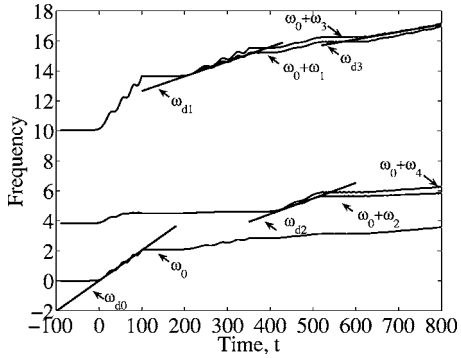

FIG. 6. The continuing phase locking in the system. The straight line segments are the drive's frequency at different stages. It is seen that at each stage the appropriate frequencies adhere to the drive's frequency, $\omega_{di} \approx \omega_0 + \omega_i$.

globally nonintegrable equation are not bound to be of the form of (6), still we seek solutions of that form. For this example we wish to excite a two-phase solution. We set, $M=7$, $\Delta=0.2$, and the following parameters were used: $\alpha_i=[0.04,0.01,0.01,0]$, $\varepsilon_i=[0.04,0.04,0.2,0]$, $\omega_{ri}=[0,16.8032,58.0223,2.7781]$, with drives changing at times $t_i=[-100,100,250,500]$. Note that at $t=500$ we stopped the drive and let the unperturbed solution evolve. Figure 7 shows the time evolution of the absolute value of one of the lattice sites. The phenomenon of synchronization threshold is present here as well, in Fig. 7 the dashed line shows the result of simulation, where the drive amplitude for excitation of the plane wave is below the threshold value ($\varepsilon^{\text{th}}=0.039$) and autoresonance does not occur. Similar results of falling out of resonance are observed in all stages of excitation.

In order to show that the numerical solution is a one-phase solution at the end of the second excitation stage ($t=250$) we examined its Fourier spectrum (not shown). In order to show that the excited solution is approximately a two-phase solution after the second excitation stage ($t>500$), we examined the Fourier spectrum of the solution, extracted from there one of the base frequencies, say ω_1, and

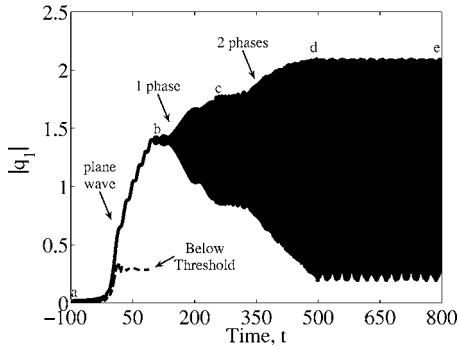

FIG. 7. Excitation of a two-phase solution in the nonintegrable case. Shown is the time evolution of $|q_1|$. The letters indicate significant time stamps, (a) application of plane wave drive, application of first (b) and second (c) phases' drives, termination of drive (d) and in the end (e). The dashed line shows the same simulation with the first drive amplitude below threshold.

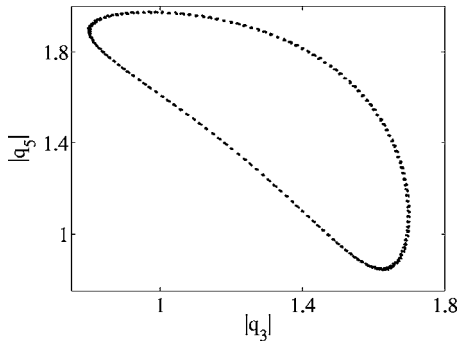

FIG. 8. Verification of the two-phase solution. The solution exhibits periodic behavior in $(|q_3|,|q_5|)$-space at discrete times $T_i=T_0+(2\pi/\omega_1)i$, ω_1 being one of the basic frequencies. The closed curve $|q_5|$ versus $|q_3|$ indicates a two-phase solution. The curve's thickness is not zero because the solution is only approximately a two-phase solution.

examined the solution at discrete times $T_i=T_0+(2\pi/\omega_1)i$, $i=0,1,\ldots$ for some arbitrary T_0. If the solution's absolute value $A_n(t)\equiv|q_n(t)|$ is truly composed of only two frequencies and their harmonics, then $A_n(T_i)$ will be a periodic discrete time series, and its phase space trajectories should be closed contours, with borders' thickness tending to zero. Figure 8 shows the result of this analysis. The arising trajectory is clearly closed, implying that the solution is approximately of two phases, but it does have a finite thickness (not related to the graphical implementation), indicating the existence of other, though much less significant, phases in the solution.

C. Synchronized discrete breathers

In this example we excite a specific type of a two-phase solution, the periodic discrete breather, which is a solution of form (6) with two phases ($m=2$), such that the time dependencies in W cancel out and the solution receives the form

$$q_n(t) = A_n e^{i\omega_0 t},$$

i.e., all the time dependence is in $\Theta_0=\omega_0 t$. Emergence of similar standing waves in a continuous NLS system by synchronization was studied previously [38] and contributed the idea of excitation of periodic breathers in discrete systems in this example. The excitation scheme for breathers is conceptually similar to that of the previous examples, yet somewhat different. In this scheme we use the driving term of the form $f_n(t)=[\varepsilon_0+\varepsilon_1\cos(k_0 n)]\exp[-i\int\omega_d(t)dt]$, $\omega_d(t)=\alpha t$, i.e., a combination of three chirped frequency plane waves, $\varepsilon_0 e^{-i\int\omega_d(t)dt}$ and $(\varepsilon_1/2)e^{\pm k_0 n - i\int\omega_d(t)dt}$. We do not analyze this scheme and the emerging solution in this work and it is a subject for further research.

We present the case of the integrable equation IDNLS ($\nu=0$). The following parameters were used in the simulation: $M=7$, $\Delta=0.5$, $\varepsilon_0=0.02$, $\varepsilon_1=0.01$, and $\alpha=0.01$, the simulation was run in the time span $[-200\ 1200]$, where at $t=1000$ the drive was switched off. The results of the simulations are presented in Fig. 9 showing the time evolution of $|q_n|$, $n=1,\ldots,7$. One sees that at time, $t\simeq 0$ a growing amplitude plane wave solution is excited. At time, $t\simeq 200$,

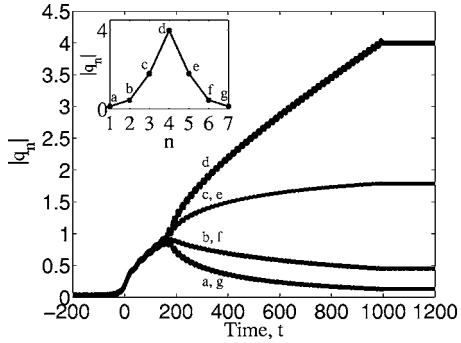

FIG. 9. The excitation of a discrete breather. The outer plot shows the time evolution of the absolute value of the solution. The inner plot depicts the absolute value of the different lattice sites in the chain in the end of the excitation process. The letters indicate which lattice site corresponds to which line.

where the plane wave's amplitude grows to a value in which this solution ceases to be stable to linear modulation (see below), a new type of solution starts to develop. This solution, the periodic discrete breather, is characterized by an absolute value which is independent of time if the driving function is turned off (see the final form of $|q_n|$ at $t=1200$ in the inner plot of Fig. 9). One sees that in the presence of the drive, the solution's absolute value slowly varies in time moving through the solutions space, as the driving perturbation causes the breather to be "steeper," or rather more localized. Once the drive is dropped, the solution is truly a discrete breather, with a constant absolute value and a real part oscillating with a constant frequency.

Further information on the excited solution is obtained by finding the evolution of the external frequency ω_0 and its main IST spectrum. The results of these computations are presented in Fig. 10. One observes a perfect phase locking in the system, as the driven solution frequency follows that of the drive continuously. The inner plot in Fig. 10 shows the main spectrum at the initial stage of excitation of the breather ($t=250$). We observe that the excited breather is a two-phase solution, since it has three pairs of nondegenerate complex conjugate spectrum components, which, in contrast to the case shown in Fig. 4(e), all lie on the imaginary axis of

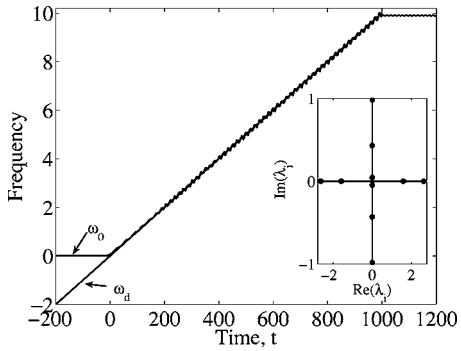

FIG. 10. Phase locking in case of a discrete breather excitation. As long as the drive is applied, ω_0 follows the drive's frequency. Once the drive is turned off ω_0 stays constant. The inner plot shows the IST spectrum of the solution at the initial stage of excitation of the breather ($t=250$).

the spectral plane. As the breather solution develops and becomes more localized, the three pairs of nondegenerate spectral points remain on the imaginary axis, while the maximal $|\mathrm{Im}\,\lambda_i|$ increases in time, the next in $|\mathrm{Im}\,\lambda_i|$ spectral point approaching the maximal point, while the minimal $|\mathrm{Im}\,\lambda_i|$ on the imaginary axis approaches zero.

The DDNLS is physically more relevant than IDNLS. Hence, of great interest are discrete breathers for the nonintegrable lattice. Whereas IDNLS has at least one well-known family of breather solutions, less is known of such solutions for periodic DDNLS and the excitation of such solutions is difficult at best [44]. Using the same excitation scheme as described above, one can excite similar periodic DDNLS breathers as well.

After illustrating our ideas in simulations, we proceed to the theory of simplest 0- and 1-phase autoresonant excitations in discrete periodic NLS systems.

III. ANALYSIS OF EXCITATION OF FLAT SOLUTIONS

In this section we study our approach to excitation of the simplest plane wave, i.e., the flat solution. Let us consider the IDNLS equation (3) first. The unperturbed equation (3) has a flat solution, $q_n(t)=a\exp(-2i\sigma a^2 t)$ for any amplitude a. We examine now the driven equation (5), where we set $f(x,t)=\varepsilon\exp(i\theta_d)$, proceed from slightly perturbed zero initial conditions, and seek solutions close to the flat solution. First, we write $q_n=a_n\exp(i\varphi_n)$, where both $a_n=a_n(t)$ and $\varphi_n=\varphi_n(t)$ are real functions, which we substitute into (5) and separate real and imaginary parts, yielding

$$\dot{a}_n=\frac{1}{\Delta^2}(a_{n+1}\sin\phi_{n+1}-a_{n-1}\sin\phi_n)+\sigma a_n^2(a_{n+1}\sin\phi_{n+1}-a_{n-1}\sin\phi_n)+\varepsilon\sin(\Theta_d-\varphi_n), \tag{7a}$$

$$-a_n\dot{\varphi}_n=\frac{1}{\Delta^2}(a_{n+1}\cos\phi_{n+1}+a_{n-1}\cos\phi_n-2a_n)+\sigma a_n^2(a_{n+1}\cos\phi_{n+1}+a_{n-1}\cos\phi_n)+\varepsilon\cos(\Theta_d-\varphi_n), \tag{7b}$$

where $\phi_n\equiv\varphi_n-\varphi_{n-1}$ and the overdot denotes a time derivative. Next, we set $a_n=a+\delta a_n$ and $\varphi_n=\varphi+\delta\varphi_n$, where a and φ are the averages over n of the amplitudes and phases, while $|\delta\varphi_n|\ll 1$, $|\delta a_n|\ll a$. We also observe that all $\phi_n=\delta\varphi_n-\delta\varphi_{n-1}$ are small and define the phase mismatch $\Phi\equiv\theta_d-\varphi$. Substituting this into Eq. (7) and linearizing yields

$$\dot{a}+\delta\dot{a}_n=\left(\frac{a}{\Delta^2}+\sigma a^3\right)(\phi_{n+1}-\phi_n)+\varepsilon\sin\Phi+\varepsilon\cos\Phi\,\delta\varphi_n, \tag{8a}$$

$$-a\dot{\varphi}-a\,\delta\dot{\varphi}_n-\delta a_n\dot{\varphi}=\frac{1}{\Delta^2}(\delta a_{n+1}+\delta a_{n-1}-2\delta a_n)+\sigma a^2(4\delta a_n+\delta a_{n+1}+\delta a_{n-1})+2\sigma a^3+\varepsilon\cos\Phi-\varepsilon\sin\Phi\,\delta\varphi_n. \tag{8b}$$

By averaging Eq. (8) over n, we can separate the n-dependent and independent parts, yielding for the n-independent variables

$$\dot{a} = \varepsilon \sin \Phi, \tag{9a}$$

$$\dot{\Phi} = -\alpha t + 2\sigma a^2 - \frac{\varepsilon}{a} \cos \Phi, \tag{9b}$$

where we have set $\dot{\theta}_d = -\alpha t$. For the n-dependent variables we have

$$\delta \dot{a}_n = \left(\frac{a}{\Delta^2} + \sigma a^3 \right) (\delta \varphi_{n+1} + \delta \varphi_{n-1}) + \left(-2\frac{a}{\Delta^2} - 2\sigma a^3 + \varepsilon \cos \Phi \right) \delta \varphi_n, \tag{10a}$$

$$-a \delta \dot{\varphi}_n = \frac{1}{\Delta^2} (\delta a_{n+1} + \delta a_{n-1} - 2\delta a_n) + \sigma a^2 (\delta a_{n+1} + \delta a_{n-1} + 2\delta a_n) + \frac{\varepsilon}{a} \cos \Phi \delta a_n - \varepsilon \sin \Phi \delta \varphi_n. \tag{10b}$$

The last four equations describe evolution and stability of the autoresonant flat solutions in our driven problem. First, we discuss the evolution of the n-independent variables a and Φ.

A. Autoresonant evolution of flat solutions

The evolution of the variables a and Φ is governed by Eqs. (9), which are also valid for the driven nonintegrable (DDNLS) case. Passage through resonance described by this pair of equations has been studied previously [34,39], and we give a short analysis here, for completeness.

1. Linear stage: Initial phase locking

Here we discuss the behavior of the solution of (9) in the initial linear excitation stage, as the solution is far enough from resonance. We define $z \equiv a e^{i\Phi}$ and rewrite (9) as a single complex equation

$$i\dot{z} + (\alpha t - 2\sigma |z|^2) z = \varepsilon. \tag{11}$$

We focus on passage through resonance, i.e., study solutions of Eq. (11) subject to zero initial conditions as the time passes the resonance at $t=0$. We shall also assume that the direction of frequency chirp is given by the sign of nonlinearity, i.e., sign α=sign σ. If the nonlinear term is neglected, the solution can be written as

$$z = -i\varepsilon \int_{t_0}^{t} e^{-(i\alpha/2)(t^2-\tau^2)} d\tau.$$

This can be integrated using Fresnel integrals, from which one can show [34] that for the linear regime, prior to the resonance ($|t| \gg \sqrt{\pi/2|\alpha|}$, $t<0$), $z \approx \varepsilon/(\alpha t)$, i.e., $a \approx \varepsilon/|\alpha t|$ and $\Phi \approx \pi$ ($\sigma=1$) or 0 ($\sigma=-1$). This indicates that the phase mismatch is trapped towards π (0). As a grows we can no longer neglect the nonlinear term and turn to examine the weakly nonlinear regime. We consider only the $\sigma=1$ ($\alpha>0$) case in the following.

2. Weakly nonlinear stage: Synchronization threshold

Entering this stage, $\Phi \approx \pi$ and we are interested in examining solutions where the phase mismatch stays around π and consequently replace $\cos \Phi \approx -1$ in Eq. (9b). We also write $a = a_0 + a_1$ where a_0 is defined as the solution of the exact phase locking equation $\dot{\Phi}=0$, or equivalently,

$$-\alpha t + 2a_0^2 - \frac{\varepsilon}{a_0} = 0. \tag{12}$$

We presume approximate phase locking, consider $|a_1| \ll |a_0|$, and expand Eq. (9) to first order in a_1 yielding

$$\dot{a}_1 = \varepsilon \sin \Phi - \frac{\alpha}{S}, \tag{13a}$$

$$\dot{\Phi} = S a_1, \tag{13b}$$

where we have defined $S \equiv 4a_0 + a_0^{-2}\varepsilon$ and used [from Eq. (12)] $\dot{a}_0 = \alpha/S$. This pair of equations forms a Hamiltonian system with Hamiltonian

$$H(a_1, \Phi) = S\frac{a_1^2}{2} + V(\Phi), \tag{14a}$$

$$V(\Phi) = \varepsilon \cos \Phi + \frac{\alpha}{S}\Phi. \tag{14b}$$

This system describes a pseudoparticle having momentum a_1 and slowly varying mass S^{-1} moving in a pseudopotential $V(\Phi)$. Entering the weakly nonlinear stage, the particle is trapped in a well with a local minimum at $\Phi \approx \pi$. As long as this stays the minimum, and variation of S is adiabatic enough (see below) the particle will continue to be trapped with the phase mismatch performing small oscillations around π, i.e., autoresonance will occur. The pseudopotential V is a tilted cosine potential, hence the condition for it to have local minima is that the tilt is smaller than the wells' depths, i.e., $\varepsilon > \alpha/S$. We recall our approximation of $\cos \Phi \approx -1$ or, equivalently, as an estimate, $|\sin \Phi| < 1/2$. Since the quasiequilibrium position is given by $\sin \Phi_0 = \alpha/(\varepsilon S)$ [see Eq. (13a)], we must satisfy $\varepsilon > 2\alpha/S$ for the validity of our approximation. From the definition of S we find the minimum value $S_{\min} = 2^{2/3} 3 \varepsilon^{1/3}$, which substituted back into the last inequality yields the necessary condition for continuing synchronization in the weakly nonlinear regime, $\varepsilon > \sqrt{2}(\alpha/3)^{3/4} = 0.62\alpha^{3/4}$. As far as the adiabaticity is concerned, we observe that the frequency of phase mismatch oscillations around the quasiequilibrium value Φ_0 in the weakly nonlinear regime is $\omega_{\rm osc} = (\varepsilon S)^{1/2}$. The adiabaticity condition $\omega_{\rm osc}^{-2} |\dot{\omega}_{\rm osc}| \ll 1$ then becomes

$$\frac{|\dot{S}|}{2\varepsilon^{1/2}S^{3/2}} = \left|\frac{\alpha S'}{2\varepsilon^{1/2}S^{5/2}}\right| \ll 1,$$

where $S' = 4 - 2\varepsilon/a_0^3$ denotes derivative of S with respect to a_0. The left-hand side in the last inequality as a function of a_0 has a maximum value of $0.078\alpha\varepsilon^{-4/3}$, which is indeed significantly less than unity for $\varepsilon > 0.62\alpha^{3/4}$, justifying the derivation of our necessary condition for capture into resonance. On the other hand, numerical solutions of Eq. (11) show that the transition to the phase locked regime by passage through resonance takes place at somewhat lower ε with a very sharp threshold, i.e., for

$$\varepsilon > \varepsilon_{\text{th}} = 0.291\alpha^{3/4}. \tag{15}$$

This sufficient condition for phase locking is just a few percent lower than the condition $\varepsilon > \alpha/S_{\min} = 0.31\alpha^{3/4}$ for existence of potential wells in $V(\Phi)$. The threshold formula was verified in full lattice simulations shown in Figs. 1 and 7.

3. Strongly nonlinear stage

Next, we consider the strongly nonlinear regime, where one assumes $a \gg \varepsilon$. For convenience we use the variable $\tilde{\Phi} \equiv \Phi - \pi$, so $\tilde{\Phi} \cong 0$. Equation (9) in this limit can be approximated as

$$\dot{a} = -\varepsilon \sin\tilde{\Phi}, \tag{16a}$$

$$\dot{\tilde{\Phi}} = -\alpha t + 2a^2. \tag{16b}$$

We separate $a = a_0 + a_1$, $\tilde{\Phi} = \tilde{\Phi}_0 + \tilde{\Phi}_1$, where a_0 and $\tilde{\Phi}_0$ are slowly varying time averages, whereas a_1 and $\tilde{\Phi}_1$ are rapidly oscillating, but small. Substituting these definitions into (16) and dividing into oscillating and nonoscillating parts yields

$$\dot{a}_0 = -\varepsilon\tilde{\Phi}_0, \quad \dot{\tilde{\Phi}}_0 = -\alpha t + 2a_0^2, \tag{17a}$$

$$\dot{a}_1 = -\varepsilon\tilde{\Phi}_1, \quad \dot{\tilde{\Phi}}_1 = 4a_0a_1. \tag{17b}$$

We seek a quasisteady state $\dot{\tilde{\Phi}}_0 = 0$ in (17a), which leads to

$$a_0 = \sqrt{\frac{1}{2}\alpha t}, \quad \tilde{\Phi}_0 = -\frac{\alpha}{4a_0\varepsilon}.$$

By differentiating (17b) again we can extract the frequency of oscillations of a_1 around the average a_0 and get $\omega_{\text{osc}} = \sqrt{4\varepsilon a_0}$. These autoresonant oscillations are clearly seen in Figs. 1 and 7 in the first stage of excitation (flat solution).

Combining Eqs. (16) and (17) leads to

$$\dot{a}_1 = -\varepsilon \sin\tilde{\Phi} - \frac{\alpha}{4a_0},$$

$$\dot{\tilde{\Phi}} = 4a_0a_1, \tag{18}$$

which is a Hamiltonian system,

$$H(a_1, \tilde{\Phi}) = 2a_0a_1^2 + V(\tilde{\Phi}),$$

$$V(\tilde{\Phi}) = -\varepsilon\cos\tilde{\Phi} + \frac{\alpha}{4a_0}\tilde{\Phi}. \tag{19}$$

Again, the necessary condition for trapping a_1 in a potential well with $|\tilde{\Phi}| < 1/2$ is

$$\varepsilon > \frac{\alpha}{2a_0} = (\alpha/2t)^{1/2},$$

meaning that the drive's amplitude can be reduced in time as the amplitude grows. One also finds that the adiabaticity condition, $\omega_{\text{osc}}^{-2}|\dot{\omega}_{\text{osc}}| \ll 1$, necessary for continuing phase locking in the system improves in the strongly nonlinear regime as the amplitude grows.

B. Stability analysis

We are now interested in finding the modulational stability region of the autoresonantly driven flat solution. For the solution to be stable we demand that δa_n and $\delta\varphi_n$ stay small and oscillating at all times. Assuming, $\delta\varphi_n = \text{Re}\{\delta\varphi \exp[i(\kappa_m n - \upsilon t)]\}$ and $\delta a_n = \text{Re}\{\delta a \exp[i(\kappa_m n - \upsilon t)]\}$, setting $\cos\Phi \approx -\sigma$, $\sin\Phi \approx 0$, and defining, for convenience, $\chi_m^{\pm} \equiv \cos(\kappa_m) \pm 1$, Eqs. (10) become

$$-i\upsilon\delta a_n = [2(a\Delta^{-2} + \sigma a^3)\chi_m^- + \sigma\varepsilon]\delta\varphi_n, \tag{20a}$$

$$i\upsilon a\,\delta\varphi_n = \left(2\Delta^{-2}\chi_m^- + 2\sigma a^2\chi_m^+ + \sigma\frac{\varepsilon}{a}\right)\delta a_n. \tag{20b}$$

This leads to the dispersion relation

$$\upsilon^2 = \frac{1}{a}[2(a\Delta^{-2} + \sigma a^3)\chi_m^- + \sigma\varepsilon]\left(2\Delta^{-2}\chi_m^- + 2\sigma a^2\chi_m^+ + \sigma\frac{\varepsilon}{a}\right), \tag{21}$$

yielding, in $\varepsilon = 0$ case, stability conditions, $a\Delta \leqslant 1$ for the defocusing case ($\sigma = -1$) and $a\Delta \leqslant \min_{m=1,\ldots,M-1}\sqrt{-\chi_m^-/\chi_m^+} = \tan(\pi/M)$ for the focusing case. For small $\varepsilon \neq 0$, $a\Delta$ may be slightly above unity in the defocusing case for stability and must lie slightly below $\tan(\pi/M)$ in the focusing case. Similar calculations for the nonintegrable DDNLS system show that the defocusing case is always modulationally stable, while the focusing state requires $a\Delta < \sin(\pi/M) + O(\varepsilon)$ for stability. We note here that unlike the continuous defocusing NLS, where the flat solution is stable for all amplitudes, in the discrete case there is a critical value a_{cr} above which the solution is unstable, though in the continuous limit $a_{\text{cr}} \to \infty$. We illustrate loss of stability of autoresonant plane waves in simulations in Fig. 11. The figure shows evolution of the absolute values $|q_n|$ in two simulations differing only by a small random modulation added to the zero initial condition. In both simulations the parameters are $M = 5$, $\Delta = 3/5$, $\alpha = 0.05$, $\varepsilon = 0.05$. One sees that the flat solutions grow up in autoresonance to their critical amplitude ($a_{\text{cr}} = 1.21$) beyond which the plane waves are destroyed and a different type of solution evolves. These emerging solutions are entirely different from each other though they are determined only by a small, random initial perturbation. It is interesting to view the breakdown of the flat wave in the IST spectrum

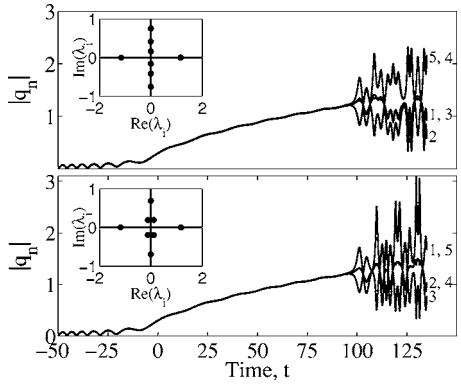

FIG. 11. Breakdown of the plane wave solution. Once the critical amplitude $a_{cr}=1.21$ is reached, the plane wave solution breaks down and a two-phase solution emerges. The shape of the two-phase solution is determined solely from a random initial perturbation. The numbers 1 through 5 indicate which line corresponds to which lattice site (some lines are double), accentuating the difference between the two emerging solutions. The inner plots show the spectra at time $t=130$ indicating that these are two-phase solutions.

space (inner plots in Fig. 11). We find that once the critical amplitude is passed there is a "collision" of two initially degenerate pairs of spectral points and two gaps are opened, yielding a two-phase solution. Hence however "chaotic" the solution may seem, it is not. Interesting to note that application of addition drives with the same frequency (as for example in Sec. II C) allows us to form a stable periodic discrete breather (also a two-phase solution) beyond the modulational instability point and autoresonantly control its shape. A similar phenomenon in the continuous NLS case was studied in Ref. [38].

IV. EXCITATION OF ONE-PHASE SOLUTIONS

A. Governing equations

In this section we seek solutions of form

$$q_n(t) = W(\theta)e^{i\xi}, \tag{22}$$

where $\theta=\kappa n-\int \omega dt$, $\kappa=2\pi m/M=mk_0$ (m being an integer), $\xi=-\int \gamma dt$, and $\omega(t),\gamma(t)$ are slow functions of time. The driving term needed to excite this one-phase solution is

$$f_1(t) = \varepsilon_1 \exp\left[i\left(\kappa n - \int \omega_d dt \right)\right] = \varepsilon_1 \exp(i\theta_d).$$

Substituting (22) into (5) yields

$$i\dot{W}_n + \gamma W_n = \frac{1}{\Delta^2}(W_{n+1}+W_{n-1}-2W_n) + \sigma|W_n|^2(W_{n+1}+W_{n-1}) + \varepsilon_1 \exp[i(\theta_d-\xi)]. \tag{23}$$

Next, we expand W in a Fourier series,

$$W(\theta) = A_0 + A_1 e^{i\theta} + B_1 e^{-i\theta} + A_2 e^{2i\theta} + B_2 e^{-2i\theta} + \cdots .$$

We consider small amplitude deviations from a plane wave solution, i.e., assume that A_n and B_n are of $O(\delta^n)$ for some small parameter δ and neglect terms of order δ^4 and higher in the evolution equation for W. We further assume that ε and the time derivatives of A_n, B_n are of $O(\delta^3)$. Now, we wish to treat $\omega(t)$ as a constant and project its time dependence onto the Fourier expansion coefficients, i.e., we define $\omega(t)=\omega_0+\omega_1(t)$, $a_n \equiv A_n \exp[-in\int \omega_1(t)dt]$, $b_n \equiv B_n \exp[+in\int \omega_1(t)dt]$ and rewrite

$$W(\theta) = a_0 + a_1 e^{i\theta_0} + b_1 e^{-i\theta_0} + a_2 e^{2i\theta_0} + b_2 e^{-2i\theta_0} + \cdots ,$$

where $\theta_0=\kappa n-\int \omega_0 dt$, and $-\dot{\theta}_0=\omega_0$ is a constant. Without loss of generality [by simply redefining phase ξ in Eq. (22)] one can view a_0 in the last equation as real and we shall adopt this convention in the following. Next, we substitute W's Fourier expansion into (23) and compare harmonics to produce the governing equations for the variables $a_i(t)$, $b_i(t)$, and $\gamma(t)$. We shall form our one-phase excitation by starting from a flat solution, so we may define $a_0=a_{00}+a_{01}$, $\gamma=\gamma_0+\gamma_1$, where a_{00} is the amplitude of the plane wave from which the one-phase excitation stage begins, $\gamma_0=2\sigma a_{00}^2$, while a_{01} and γ_1 are assumed to be of $O(\delta^2)$ (to be seen later). Also, we use the notations, $\alpha_1=-4\sin^2(\kappa/2)$, $\alpha_2=-4\sin^2\kappa$, $\alpha_3=2\cos\kappa$, $\alpha_4=2\cos(2\kappa)$, and $\alpha_5=2\cos^2(\kappa/2)$ in the following.

1. First harmonic, $O(\delta^1)$

The equations arising from comparing the $\exp(\pm i\theta_0)$ terms in (23) up to $O(\delta)$ are

$$\gamma_0 b_1 + a_1^*\left(\frac{\alpha_1}{\Delta^2}+\frac{1}{2}\gamma_0\alpha_3-\omega_0\right)=0, \tag{24a}$$

$$\gamma_0 a_1 + b_1^*\left(\frac{\alpha_1}{\Delta^2}+\frac{1}{2}\gamma_0\alpha_3+\omega_0\right)=0. \tag{24b}$$

This leads to the linear dispersion relation,

$$\omega_0 = \sqrt{x_1^2-4a_{00}^4}, \quad x_1 \equiv -\alpha_1\Delta^{-2}-\sigma a_{00}^2\alpha_3, \tag{25}$$

and the relation,

$$b_1 = c_1 a_1^*, \quad c_1 \equiv \frac{x_1+\omega_0}{2\sigma a_{00}^2}. \tag{26}$$

2. Zeroth harmonic and conservation law

The zeroth harmonic equation from (23) is

$$a_0\{-\gamma+2\sigma[a_0^2+\alpha_5(|a_1|^2+|b_1|^2)]\}+2\sigma\alpha_3 a_0^* a_1 b_1 = 0. \tag{27}$$

In order to proceed from here we need another equation, a conservation law. One can show (see Appendix B) that the quantity $a_0^2/\cos\kappa+2|b_1|^2$ is conserved even with the driving term, and using the initial conditions we get

$$\frac{a_0^2}{\cos\kappa}+2|b_1|^2=\frac{a_{00}^2}{\cos\kappa}. \tag{28}$$

Combining (26)–(28) we find the corrections for a_{00} and γ_0,

$$a_0 = a_{00}+\bar{a}|a_1|^2, \quad \gamma = 2\sigma a_{00}^2+\bar{\gamma}|a_1|^2. \tag{29}$$

(see Appendix B for expressions for constants $\bar{a}$ and $\bar{\gamma}$).

3. Second harmonic, $O(\delta^2)$

Equating $\exp(\pm 2i\theta)$ terms in (23) and retaining terms up to $O(\delta^2)$ yields

$$2\sigma a_{00}^2 b_2^* + \sigma a_{00}(\alpha_3 a_1^2 + 2\alpha_5 a_1 b_1^*) + a_2(\alpha_2\Delta^{-2} - \gamma + \sigma a_{00}^2\alpha_3^2 - 2\omega_0) = 0, \quad (30a)$$

$$2\sigma a_{00}^2 a_2^* + \sigma a_{00}(\alpha_3 b_1^2 + 2\alpha_5 a_1^* b_1) + b_2(\alpha_2\Delta^{-2} - \gamma + \sigma a_{00}^2\alpha_3^2 + 2\omega_0) = 0, \quad (30b)$$

which, using the previous equations, become

$$b_2 = c_2 a_1^{*2}, \quad a_2 = c_3 a_1^2, \quad (31)$$

where constants $c_{2,3}$ are given in Appendix B.

4. First harmonic, $O(\delta^3)$

Now, we examine the first harmonic up to the third order in δ. Here we must retain the time derivatives and the driving term, but only in the $\exp(+i\theta)$ terms' equation. Indeed, since we are examining the situation where the driving term's phase, $\theta_d - \xi$, passes through θ, yielding slow phase mismatch $\theta_d - \xi - \theta$ when these two phases are locked (the desired autoresonant state). In contrast, the $\exp(-i\theta)$ terms' equation yields driving term with rapidly varying phase $\theta_d - \xi + \theta$, which we neglect in the following. This comprises the single resonance approximation in our theory. The resulting equations, after some algebra can be written as

$$i\dot{a}_1 + (x_1 + \omega_0)a_1 = c_4|a_1|^2 a_1 + 2\sigma a_{00}^2 b_1^* + \varepsilon_1 \exp[i(\theta_d - \xi - \theta)], \quad (32a)$$

$$-i\dot{b}_1^* + (x_1 - \omega_0)b_1^* = c_5|b_1|^2 b_1^* + 2\sigma a_{00}^2 a_1, \quad (32b)$$

where constants $c_{4,5}$ are given in Appendix B.

This pair of equations concludes the set of governing equations in the problem. We note that Eqs. (32) govern the behavior of the variables a_1 and b_1 and Eqs. (29) and (31) give a_0, γ, a_2, b_2 as functions of a_1 and b_1, so understanding the behavior Eq. (32) is what is necessary to understand the entire system at this stage.

B. Analysis of governing equations

First, we rewrite Eqs. (32) in vector form

$$i\tilde{\mathbf{I}}\cdot\dot{\mathbf{V}} + \mathbf{M}\cdot\mathbf{V} + \mathbf{H} + \mathbf{\Sigma} = \mathbf{0}, \quad (33)$$

where $\tilde{\mathbf{I}} \equiv \left(\begin{smallmatrix} 1 & 0 \\ 0 & -1 \end{smallmatrix}\right)$ and other vectors and matrices are defined as

$$\mathbf{V} \equiv \begin{pmatrix} a_1 \\ b_1^* \end{pmatrix}, \quad \mathbf{M} \equiv \begin{pmatrix} x_1 + \omega_0 & -2\sigma a_{00}^2 \\ -2\sigma a_{00}^2 & x_1 - \omega_0 \end{pmatrix},$$

$$\mathbf{H} \equiv -\begin{pmatrix} c_4|a_1|^2 a_1 \\ c_5|b_1|^2 b_1^* \end{pmatrix}, \quad \mathbf{\Sigma} \equiv -\begin{pmatrix} \varepsilon_1 \\ 0 \end{pmatrix} e^{i(\theta_d - \xi - \theta)}.$$

We wish to analyze this equation perturbatively. To do so we introduce the parameter $\beta \ll 1$, describing the slowness of evolution of $\mathbf{V}$ and view both the driving and the nonlinear terms as $O(\beta)$. We expand $\mathbf{V}$ in powers of parameter β, $\mathbf{V} = \mathbf{V}_0 + \mathbf{V}_1 + \cdots$. Next, we observe that $\mathbf{M}$'s eigenvalues are $\lambda_{1,2} = 0, 2x_1$. The eigenvector corresponding to $\lambda_1 = 0$ is

$$\mathbf{e_1} = \frac{1}{\sqrt{2x_1}}\begin{pmatrix} \sqrt{x_1 - \omega_0} \\ \sqrt{x_1 + \omega_0} \end{pmatrix} \equiv \begin{pmatrix} \sqrt{\rho_-} \\ \sqrt{\rho_+} \end{pmatrix}.$$

$\mathbf{M}$'s symmetry allows us to write, $\mathbf{M} = \lambda_1 \mathbf{e_1}\mathbf{e_1}^T + \lambda_2 \mathbf{e_2}\mathbf{e_2}^T = \lambda_2 \mathbf{e_2}\mathbf{e_2}^T$. To zeroth order $\mathbf{M}\cdot\mathbf{V}_0 = \mathbf{0}$, hence $\mathbf{V}_0$ is an eigenvector and we may rewrite, $\mathbf{V}_0 = \zeta_1 \mathbf{e_1} + \zeta_2 \mathbf{e_2}$. Since its eigenvalue is 0, we deduce $\zeta_2 = 0$, $\zeta_1 \neq 0$. Returning to (33) and expanding to order β yields

$$i\tilde{\mathbf{I}}\cdot\dot{\mathbf{V}}_0 + \mathbf{M}\cdot\mathbf{V}_1 + \mathbf{H}^0 + \mathbf{\Sigma} = \mathbf{0},$$

where $\mathbf{H}^0 = -(c_4|a_{10}|^2 a_{10}, c_5|b_{10}|^2 b_{10}^*)^T$. Multiplying this from the left by $\mathbf{e_1}^T$ and rewriting explicitly leads to

$$i\dot{\zeta}_1 = c_6|\zeta_1|^2\zeta_1 + \tilde{\varepsilon}\exp[i(\theta_d - \xi - \theta)], \quad (34)$$

where $\tilde{\varepsilon} = (x_1/\omega_0)\sqrt{\rho_-}\varepsilon_1$, and constant c_6 is given in Appendix B. Writing $\zeta_1 = Ae^{i\eta}$ for real A and η, substituting into (34) and separating real and imaginary parts yields

$$\dot{A} = \tilde{\varepsilon}\sin\phi, \quad (35a)$$

$$\dot{\phi} = -\sigma|\alpha|t + c_7 A^2 + \frac{\tilde{\varepsilon}}{A}\cos\phi, \quad (35b)$$

where c_7 is given in Appendix B, we have defined phase mismatch $\phi \equiv \theta_d - \xi - \theta - \eta$, considered the driving frequency of form $\omega_d = -\dot{\theta}_d = \omega_r + \alpha t$, and set $\alpha = \sigma|\alpha|$. This pair of equations is similar to Eqs. (9), hence we can draw the conclusion that the phenomenon of autoresonance does occur in this system and that the threshold for autoresonance is

$$\varepsilon_1^{\text{th}} = c_8|\alpha|^{3/4} = 0.411\frac{\omega_0}{x_1}\frac{1}{\sqrt{\sigma\rho_- c_7}}|\alpha|^{3/4}. \quad (36)$$

Yet, what does autoresonance mean in terms of the original phase variables? We note that in a weakly excited stage $\mathbf{e_1}^T\mathbf{V}_0 \cong \zeta_1$, meaning $\zeta_1 \approx \sqrt{\rho_-}a_1 + \sqrt{\rho_+}b_1^*$, hence ζ_1's phase η is none other than $-\int\omega_1 dt$. Therefore, the phase locking condition $\phi \approx \pi$ becomes $\theta_d - \xi - \int(\omega_0 + \omega_1)dt = \theta_d - \xi - \theta \approx \pi$, and the original variable's (W's) phase is locked to the difference between the driving and the external phases. As for the evolution of the amplitude of W, only qualitative insights are possible. The expected autoresonant growth of ζ_1's amplitude indicates a growth in the amplitude of a_1 and b_1. This, in turn, implies [using Eq. (31)] a growth also in a_2 and b_2. The behavior of the last variable, a_0, is determined from the conservation law (28), which implies that for an excitation of a mode κ_m such that $\cos\kappa_m < 0$, a_0 will also grow and so also the wave's average amplitude. If, however, we excite a phase with κ_m such that $\cos\kappa_m > 0$, a_0 will decrease, bringing about a wave with a decreasing lower envelope of $|W|$.

To sum up, while starting from a situation where W is a constant, after passage through resonance W becomes a function $W = W(\theta)$ where phase $\theta + \xi$ is locked to that of the drive. In short, application of a driving force like f_1 with an ampli-

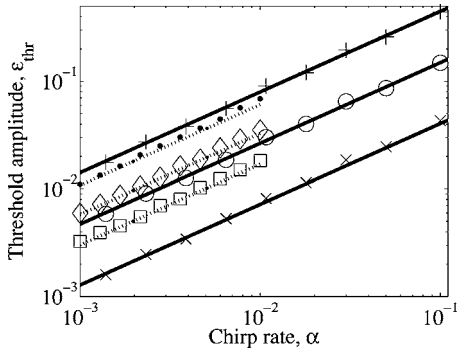

FIG. 12. Numerically determined threshold drive amplitude for excitation of a one-phase solution from a plane wave as a function of the chirp rate, versus theoretical predictions. The solid lines (theory) represent the integrable case, $M=4$, $\Delta=0.5$ for different plane wave amplitudes $a_{00}=0.8, 1.3, 1.8$, (+, ○, and × in simulations), the dashed lines (theory) represent the nonintegrable case for $M=7$, $\Delta=2/7$ and amplitudes $a_{00}=0.8, 1.0, 1.2$, (·, ◇, and □ in simulations). In all cases the scaling $\varepsilon_{\text{th}} \sim \alpha^{3/4}$ is the same, but with different proportion constants.

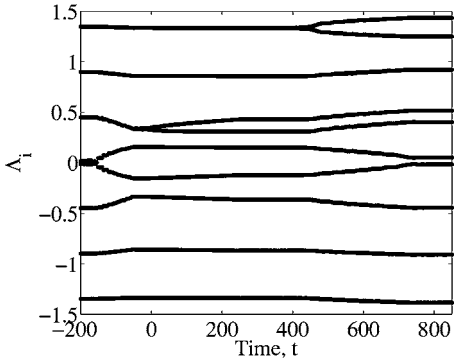

FIG. 13. The time evolution of the associated DDNLS spectra. Derived by adiabatically changing the discretization parameter ν from 1 to 0 and calculating the main spectrum of the emerging IDNLS solution.

tude greater than $\varepsilon_1^{\text{th}}$ will autoresonantly excite a one-phase solution. We note here that for the nonintegrable case, similar calculations may be carried out leading to a result the same as this result, where we set $\alpha_3 \to 2$, $\alpha_4 \to 2$, $\alpha_5 \to 2$ in all the constants.

A verification of the threshold theory is illustrated in Fig. 12, which shows the numerically found drive amplitude threshold ε_{th} as a function of the chirp rate α, versus a theoretical prediction. For this example we used $M=4$, $\Delta=0.5$ for $\nu=0$ (integrable case), $M=7$, $\Delta=2/7$ for $\nu=1$, and examined the theoretical prediction versus numerical results for a range of chirp rates between 10^{-3} and 10^{-1}. We repeated this procedure for three different amplitudes a_{00} of the initial plane wave. The scaling of $\varepsilon_{\text{th}} \sim \alpha^{3/4}$ does not depend on a_{00}, but the proportion constant does. The numerical derivation of the threshold amplitude was done by a simple binary search procedure, where the initial guess used was the theoretical prediction. The determination whether a solution is in autoresonance was done by checking the phase locking between the drive and the solution. This, in turn, was done by the following method. For every solution we checked the quantity $S \equiv \Sigma[\omega_d - (\gamma+\omega)]\Delta t \approx \int_0^{t_f}[\omega_d - (\gamma+\omega)]dt$, where Δt is the discrete time step and t_f is the time the simulation was stopped. If the solution is phase locked with the drive, $|S|$ is bounded for arbitrary choice of t_f. If, however, the solution is not phase locked and the frequency sum $\gamma+\omega$ ceases to grow from a certain time (near $t=0$), then $S \approx (\alpha/2)t_f^2$ (the area of the triangle trapped between the curves ω_d and $\gamma+\omega$). The difference between these quantities (for any time span that is not very small) is usually of at least two orders of magnitude. So the evaluation of S and checking if $S < C\alpha t_f^2$ for some small C is a good numerical method to check for phase locking. We add here that the validity of this theory for the nonintegrable case requires working with sufficiently small excitations (see Sec. V), so for this case we are bounded to examine only smaller chirp rates.

V. EXCITATION OF MULTIPHASE SOLUTIONS IN NONINTEGRABLE CASE

In the preceding sections we presented an excitation procedure and developed a theory to analyze and explain the emerging results for the IDNLS. We also applied the same numerical excitation scheme to DDNLS, ignoring its nonintegrability. This approach proved quite successful. We were able to excite multiphase solutions and received predictions for the threshold phenomenon which were quite accurate. In this section we wish to focus on DDNLS, describe a diagnostics tool for the DDNLS based on IST ideas, and discuss the validity of application of autoresonant control of solutions of this globally nonintegrable system.

First, we wish to analyze a given autoresonant DDNLS solution and show that it is approximately an n-phase solution, which is phase locked with the driver. To do so we note that autoresonance is a phenomenon in which the phase locking is persistent to adiabatic changes not only in the external drive's frequency but also to adiabatic changes in the system's parameters. Consequently, a sufficiently slow change of parameter ν [see Eq. (2)] from 1 to 0 which leads from a (nonintegrable) DDNLS system to an integrable IDNLS equation (where we have IST analysis at our disposal), does not destroy the phase locking property of the system. Therefore, given a driven solution of DDNLS at a given time and adiabatically changing ν to 0 (while keeping a constant driving frequency), analyzing the solution in the end of this process and receiving an IDNLS solution that is phase locked with the drive and has say, n, excited phases, means that the original system was approximately an n-phase DDNLS solution phased locked with the drive. In practical terms this approach to analyzing autoresonant DDNLS excitations works as follows. We take a driven DDNLS solution (referred to as the original solution), and at a specific set of (equally spaced) times, t_i $i=1,2,\ldots$ use this solution as initial conditions for simulations, where the drive's frequency remains constant and ν is slowly varied from 1 to 0. At the end of these multiple adiabatic transitions to IDNLS we calculate the IST spectra of the resulting IDNLS solutions. We refer to this set of spectra as the DDNLS solution's associated spectra $\{\lambda(t_i)\}$. Figure 13 shows the associated spectra

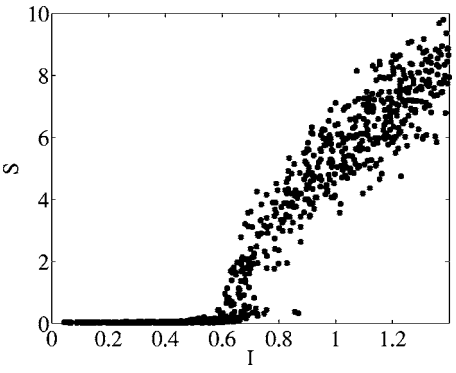

FIG. 14. The area S trapped under the power spectrum curve versus the average $I=[(1/M)\Sigma_n|q_n|^2]^{1/2}$. Small S indicates discrete line power spectra characteristic of a quasiperiodic solution, while larger S characterize continuous power spectra in the case of the chaotic behavior. There is a critical value $I_c \approx 0.55$ below which chaos is not observed.

for an example with $M=7$, $\Delta=0.2$, where we attempted to excite a two-phase DDNLS solution. We use the $\Lambda=\mathrm{Re}\,\lambda+0.5\,\mathrm{Im}\,\lambda$ representation of the spectrum in the figure for better exposition of the time evolution (similar to that in Fig. 5). We observe that the associated spectrum shows successive opening of three gaps indicating that there are 0, 1, and 2 excited phases in the original autoresonant DDNLS solution at the appropriate times.

Next, we discuss the integrability of DDNLS system. Our ability to excite a variety of autoresonant solutions (as in the examples in Sec. II and above) in this system indicates integrability in certain parameter range, but does not mean global integrability in this system. Indeed, under certain conditions, DDNLS exhibits chaotic behavior [13], but exhibits integrability under other conditions. For example, for the case $|q_n| \ll 1$ DDNLS is nearly linear and is integrable. Furthermore, we have found numerically that given the average $I^2=(1/M)\Sigma_n|q_n|^2$, as long as $I^2<I_c^2$ for some I_c, DDNLS exhibits regular behavior. This is illustrated in Fig. 14. We choose initial conditions of the form $q_n=\Sigma_m c_m \exp(i\kappa_m n)$, with some choice of c_m and allowed an unperturbed DDNLS solution to evolve. Then we analyzed the Fourier spectrum of the solution. We calculated the area $S\equiv\int_0^\infty|\hat{q}_1|^2(\omega)d\omega$ trapped under the Fourier spectrum curve on the first lattice cite, where the largest peak was normalized to unity. For an integrable system $S\to 0$ as the spectrum exhibits sharp peaks corresponding to the discrete frequencies, whereas for a chaotic system, there are continuum bands in the spectrum, the area trapped underneath which does not tend to zero. We have repeated this calculation for many (10^3) random sets of c_m and show the resulting values of S in Fig. 14 as a function of I for the example $M=7$, $\Delta=3/7$ and $m=1,2$ (first two lowest order modes) in the initial conditions. There is a clear critical value above which chaotic behavior is observed and under which there is no chaotic behavior. Since multiphase autoresonance requires existence of well-defined frequencies in the driven system, we interpret the existence of integrability regime for $I<I_c$ as being the main reason for successful formation of multiphase autoresonant DDNLS excitations satisfying this condition.

VI. CONCLUSIONS

In conclusion, (a) we presented an autoresonant excitation scheme of multiphase solutions in discrete nonlinear Schrödinger systems by starting from zero initial conditions. This scheme involves successive application of simple small amplitude plane-wave-type driving terms with slowly varying frequency. The multiphase solution is achieved by successive formation of phases in the driven solution.

(b) The excitation of each phase is based on pattern formation by synchronization (autoresonance) approach, whereby a chirped frequency drive slowly passes through the particular phase's resonant frequency. The system is resonantly excited by the drive initially and then continuously adjusts itself to the drive's frequency, keeping it always in resonance with the drive, and thus is completely controlled by the externally applied perturbation.

(c) We demonstrated the application of the above-mentioned scheme in both integrable and nonintegrable cases. We showed a stable autoresonant growth of nonlinear waves in those systems and established the phase locking property using IST analysis. We also illustrated the applicability of our scheme for excitation and control of a specific type of two-phase solutions, the periodic discrete breathers.

(d) We developed a theory for the excitation of 0- and one-phase solutions.

(e) Our theory predicts a threshold phenomenon, whereby given a chirp rate α there is a sharp threshold for the drive's amplitude for autoresonance to occur. The scaling of this threshold phenomenon is $\varepsilon \sim |\alpha|^{3/4}$. We received excellent agreement between our theory's prediction and numerical results.

(f) Our theory predicts a scaling $\omega_{\mathrm{osc}} \sim \sqrt{\varepsilon}$ of the frequency ω_{osc} of oscillating modulations of the locked frequency (or sum of frequencies) around the drive's frequency. This is numerically observed.

(g) Our analytic theory is limited to 0- and 1-phase excitations and is mainly based on the weakly nonlinear stage of excitation. However, numerically, we have shown that the waves' evolution continues into a strongly nonlinear regime as well. We have also successfully applied our excitation scheme to a larger number of excited phases in the solution and proved autoresonant phase locking by either the spectral IST analysis for the integrable case or via Fourier analysis.

(h) We developed an indirect tool for the analysis of autoresonant DDNLS solutions, using the IST approach, by exploiting the persistence of autoresonance to adiabatic change in the system's parameters. We have, furthermore, studied a numerical criterion for the evasion of chaotic behavior in this nonintegrable system.

(i) Finally, it is important to develop a general theory (probably within the IST approach) of multiphase autoresonance in IDNLS system in the future. The extension of multiphase autoresonant excitation and control ideas to other discrete integrable and nonintegrable systems also seems to be an important goal for future research.

ACKNOWLEDGMENTS

This work was supported by Israel Science Foundation (Grant No. 187/02), INTAS (Grant No. 03-51-4286), and

RFBR (Grant No. 03-02-16350).

APPENDIX A: SPECTRAL THEORY OF IDNLS

In this section, we give a precise of the spectral theory of the inverse scattering transform for IDNLS (3), for a full description see Refs. [1,17,19]. The linear scattering problem associated with IDNLS is

$$\vartheta_{n+1} = F_n \vartheta_n, \quad \frac{\partial \vartheta_n}{\partial t} = G_n \vartheta_n, \tag{A1}$$

where ϑ_n is a two-component vector and, for the focusing equation case ($\sigma = +1$)

$$F_n = \begin{pmatrix} z & q_n \Delta \\ -q_n^* \Delta & \bar{z} \end{pmatrix},$$

$$G_n = \frac{i}{\Delta^2} \begin{pmatrix} -\frac{1}{2}(z-\bar{z})^2 - \Delta^2 q_n q_{n-1}^* & -\Delta(z q_n - \bar{z} q_{n-1}) \\ -\Delta(\bar{z} q_n^* - z q_{n-1}^*) & \frac{1}{2}(z-\bar{z})^2 + \Delta^2 q_n^* q_{n-1} \end{pmatrix},$$

where z is a parameter and $\bar{z} = 1/z$. With these definitions for the compatibility condition

$$\frac{\partial F_n}{\partial t} = G_{n+1} F_n - F_n G_n, \tag{A2}$$

to be satisfied, $q_n(t)$ must satisfy IDNLS.

From here, one defines the monodromy matrix (the arrow shows the order of the increase of the indices in the product),

$$H_n = \prod_{j=0}^{\overleftarrow{N}} F_{n+j}, \tag{A3}$$

where we have introduced the notation $N = M - 1$.

Writing H_n as,

$$H_n = \frac{1}{z^M} \begin{pmatrix} \phi_n + f_n & -g_n \\ h_n & \phi_n - f_n \end{pmatrix}, \tag{A4}$$

one may define, $P(z^2) \equiv f_n^2 - g_n h_n$, which is a polynomial in z^2, and show that P is independent of both n and t, i.e., its roots are absolute constants. We rewrite,

$$P(z^2) = \tilde{P} \prod_{j=0}^{2M} (z^2 - E_j),$$

so that E_j are constants. The set $\{E_j\}_1^{2M}$ is referred to as the main spectrum in the following. In the focusing case ($\sigma = 1$), the symmetry of H_n implies that if z^2 is a root of P then so is $1/z^{*2}$ and so the set of $2M$ parameters E_j may be regarded as M pairs of spectral values, each consisting of two values, denoted $E_1^{(1)}$ and $E_1^{(2)}$, satisfying

$$E_1^{(1)} = R_1 e^{i\phi_1}, \quad E_1^{(2)} = R_2 e^{i\phi_2},$$

$$\phi_1 = \phi_2, \quad R_1 R_2 = 1. \tag{A5}$$

For diagnostic purposes in the body of the paper we use a different set of conserved parameters $\{\lambda_j\}_1^{2M}$ defined as $\lambda_j \equiv 2i \ln(E_j)$ $\forall j$. Obviously, λ_j comprise a set of M pairs of complex conjugate numbers.

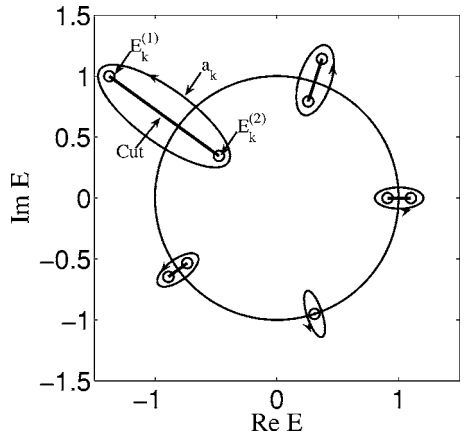

FIG. 15. Integration contours in the E space.

Next, we seek a polynomial form for f_n, g_n, and h_n. Of particular importance are the roots of g_n and we write

$$g_n = z\tilde{g} \prod_{j=1}^{N} [z^2 - \mu_j(n,t)]. \tag{A6}$$

From here one may conduct calculations leading to the recursion relation [19]

$$q_{n-1}(t) = q_n(t) \left((-1)^N \prod_{j=1}^{N} \mu_j(n,t) \right). \tag{A7}$$

Further calculations [19] yield algebraically complicated equations, which, for our purpose, can simply be written as

$$d(\ln q_n)/dt = F(\boldsymbol{\mu}), \tag{A8}$$

where $\boldsymbol{\mu} \equiv (\mu_1, \mu_2, \ldots, \mu_N)$, and F are some functions of $\boldsymbol{\mu}$. The set $\boldsymbol{\mu}$ will be referred to as the auxiliary spectrum, and its motion is governed by the dynamical equations,

$$\frac{\partial \mu_j}{\partial t} = -\frac{i}{\Delta^2} \frac{\sqrt{P(\mu_j)}[1 - (-1)^N \prod_{l \neq j} \mu_l]}{f_n^{(N+1)} \prod_{l \neq j} (\mu_j - \mu_l)}, \tag{A9}$$

where $f_n^{(N+1)}$ is the coefficient of the largest power of z^2 in the polynomial f_n. This is a complicated system of equations, but qualitative insights into the behavior of the auxiliary spectrum can be made following the technique described in Ref. [19].

We define the Riemann surface $R^2(E) = \prod_{j=1}^{2M} (E - E_j)$ and N Abelian differentials

$$du_\nu = \frac{c_{\nu 1} E^{N-1} + \cdots + c_{\nu N}}{R(E)} dE.$$

Here coefficients $c_{\mu\nu}$ are defined via normalization conditions $\oint_{a_k} du_\nu = \delta_{\nu k}$, where a_k are closed contours in the complex E-plane with cuts as shown in Fig. 15. We also define functionals,

$$l_j(\boldsymbol{\mu}) \equiv -\sum_{k=1}^{N} \int^{\mu_k} du_j = -\sum_{l=1}^{N} c_{jl} \sum_{k=1}^{N} \int^{\mu_k} \frac{E^{l-1}}{R(E)} dE, \tag{A10}$$

which have a very simple t and n dependence [19],

$$\Theta_j \equiv 2\pi l_j(\boldsymbol{\mu}) = \frac{2\pi i}{\Delta^2}(c_{j1} + c_{jN})t + \kappa_j n + \text{const.} \tag{A11}$$

The variable Θ_j is the jth phase of our multiphase solution, while $\omega_j = -2\pi i \Delta^{-2}(c_{j1} + c_{jN})$ are the frequencies. The solution is obtained by using Jacobi inversion of (A10) which leads to the relation $\boldsymbol{\mu} = \boldsymbol{\mu}(\boldsymbol{\Theta})$, meaning that $\boldsymbol{\mu}$ is a multiphase function which is 2π-periodic with respect to all its arguments Θ_j. But, according to Eq. (A8), $d(\ln q_n)/dt$ is a function of $\boldsymbol{\mu}$ only and, therefore, by substituting $q_n = |q_n| e^{i\phi_n}$,

$$d \ln(q_n)/dt = d \ln|q_n|/dt + i d\phi_n/dt = F[\boldsymbol{\mu}(\boldsymbol{\Theta})].$$

This gives $|q_n| = F_1(\boldsymbol{\Theta})$ and $d\phi_n/dt = \text{Im}[F(\boldsymbol{\Theta})] = F_2(\boldsymbol{\Theta})$, so that $\phi_n = \kappa_0 n + \omega_0 t + F_3(\boldsymbol{\Theta})$, where F_i denote some functions of the phases. From here we deduce the general form of the solution,

$$q_n(t) = F_1(\boldsymbol{\Theta}) e^{i\{\kappa_0 n + \omega_0 t + F_3(\boldsymbol{\Theta})\}} = W(\boldsymbol{\Theta}) e^{i(\kappa_0 n + \omega_0 t)}.$$

APPENDIX B: DEFINITION OF CONSTANTS AND CONSERVATION LAW

In this Appendix we summarize and explicitly write all constants used in the body of the work. We introduce the notations $\alpha_1 = -4\sin^2(\kappa/2)$, $\alpha_2 = -4\sin^2\kappa$, $\alpha_3 = 2\cos\kappa$, $\alpha_4 = 2\cos(2\kappa)$, and $\alpha_5 = 2\cos^2(\kappa/2)$. The constants used in the body of the paper are defined as follows:

(1) $x_1 = -\Delta^{-2}\alpha_1 - \sigma\alpha_3 a_{00}^2$,
(2) $\omega_0 = \sqrt{x_1^2 - 4a_{00}^4}$,
(3) $c_1 = x_1 + \omega_0/2\sigma a_{00}^2$,
(4) $\bar{\gamma} = \sigma[2\alpha_5 + (2-\alpha_3)c_1^2 + 2\alpha_3 c_1]$,
(5) $\bar{a} = -\alpha_3 c_1^2/2a_{00}$,
(6) $c_2^n = \sigma a_{00}[2\sigma a_{00}^2(\alpha_3 + 2c_1\alpha_5) - c_1(2\alpha_5 + c_1\alpha_3)(\alpha_2\Delta^{-2} + \sigma a_{00}^2\alpha_4 - 2\omega_0)]$,
(7) $c_2^d = \alpha_2^2\Delta^{-4} + a_{00}^4(\alpha_4^2 - 4) + 2\alpha_2\Delta^{-2}a_{00}^2\alpha_4\sigma - 4\omega_0^2$,
(8) $c_2 = c_2^n/c_2^d$,
(9) $c_3^n = \sigma a_{00}[2\sigma a_{00}^2(c_1^2\alpha_3 + 2c_1\alpha_5) - (2\alpha_5 c_1 + \alpha_3)(\alpha_2\Delta^{-2} + \sigma a_{00}^2\alpha_4 + 2\omega_0)]$,
(10) $c_3^d = c_2^d$,
(11) $c_3 = c_3^n/c_3^d$,
(12) $c_4 = -\bar{\gamma} + \sigma\alpha_3 + \sigma 2c_1^2\alpha_3 + \sigma a_{00}\{2\bar{a}(2\alpha_5 + 2c_1) + c_3\alpha_3^2 + c_1[2c_2\alpha_5 + c_3(\alpha_3 + \alpha_4)]\}$,
(13) $c_5 = \sigma\alpha_3 + \sigma a_{00}/c_1^3[4\bar{a} + 2c_3\alpha_5 + c_2(\alpha_3 + \alpha_4)] + c_1^{-2}\{-\bar{\gamma} + \sigma[2\alpha_3 + a_{00}(4\bar{a}\alpha_5 + c_2\alpha_3^2)]\}$,
(14) $\rho_\pm = x_1 \pm \omega_0/2x_1$,
(15) $c_6 = -x_1/\omega_0(c_4\rho_-^2 + c_5\rho_+^2)$,
(16) $c_7 = c_6 + \rho_-\bar{\gamma}$,
(17) $c_8 = 0.411\omega_0/x_1(c_7\sigma\rho_-)^{-1/2}$,
(18) $\tilde{\varepsilon} = x_1/\omega_0\sqrt{\rho_-}\varepsilon$.

The conservation law is derived as follows. Revisiting Eq. (24), this time retaining the driving term for the resonant equation (24a) and the time derivatives yields

$$i\dot{a}_1 = (-x_1 - \omega_0)a_1 + 2\sigma a_0^2 b_1^* + \varepsilon\exp(i\phi), \tag{B1a}$$

$$i\dot{b}_1 = (-x_1 + \omega_0)b_1 + 2\sigma a_0^2 a_1^*. \tag{B1b}$$

By multiplying (B1a) by a_1^* and then subtracting the complex conjugate of (B1a) multiplied by a_1 and doing the same with (B1b) and b_1, one finds

$$i\frac{d|a_1|^2}{dt} = 2\sigma a_0^2(a_1^* b_1^* - a_1 b_1) + 2i\varepsilon A\sin\phi', \tag{B2a}$$

$$i\frac{d|b_1|^2}{dt} = 2\sigma a_0^2(a_1^* b_1^* - a_1 b_1), \tag{B2b}$$

where $A = |a_1|$, $\phi' = \phi - \arg a_1$, such that $2iA\sin\phi' = a_1^*\exp(i\phi) - a_1\exp(-i\phi)$. Adding and subtracting these two equations leads to

$$\frac{d}{dt}(|a_1|^2 + |b_1|^2) = -4i\sigma a_0^2(a_1^* b_1^* - a_1 b_1) + 2\varepsilon A\sin\phi', \tag{B3a}$$

$$\frac{d}{dt}(|a_1|^2 - |b_1|^2) = 2\varepsilon A\sin\phi'. \tag{B3b}$$

Next, revisiting Eq. (27), retaining the time derivative yields

$$i\dot{a}_0 = Ra_0 + 4\sigma a_1 b_1 a_0\cos\kappa, \tag{B4}$$

where $R = -\gamma + 2\sigma[a_0^2 + 2\cos^2(\kappa/2)](|a_1|^2 + |b_1|^2)]$, which leads to

$$\frac{d}{dt}\left(\frac{a_0^2}{\cos\kappa}\right) = 4i\sigma a_0^2(a_1^* b_1^* - a_1 b_1).$$

We replace the right-hand side of this equation by an expression from (B3a), leading to

$$\frac{d}{dt}\left(\frac{a_0^2}{\cos\kappa} + |a_1|^2 + |b_1|^2\right) = 2\varepsilon A\sin\phi'.$$

Finally, using (B3b), we obtain the conservation law,

$$\frac{d}{dt}\left(\frac{a_0^2}{\cos\kappa} + 2|b_1|^2\right) = 0. \tag{B5}$$

We also note that Eqs. (B1) hold for the nonintegrable case as well. Equation (B4), however, must be slightly modified in this case by setting $\cos\kappa \to 1$, yielding

$$\frac{d}{dt}(a_0^2 + 2|b_1|^2) = 0. \tag{B6}$$

[1] M. J. Ablowitz, B. Prinari, and A. D. Trubatch, *Discrete and Continuous Nonlinear Schrödinger Systems* (Cambridge University Press, Cambridge, England, 2004).
[2] D. N. Christodoulides and R. I. Jospeh, Opt. Lett. **13**, 794 (1988).
[3] H. S. Eisenberg, Y. Silberberg, R. Morandotti, and J. S. Aitchison, Phys. Rev. Lett. **85**, 1863 (2000).
[4] W. Krolikowski and Y. S. Kivshar, J. Opt. Soc. Am. B **13**, 876 (1995).
[5] J. Meier, G. I. Stegeman, Y. Silberberg, R. Morandotti, and J. S. Aitchison, Phys. Rev. Lett. **93**, 093903 (2004).
[6] A. S. Davydov, J. Theor. Biol. **38**, 559 (1973).
[7] F. Kh. Abdullaev, B. B. Baizakov, S. A. Darmanyan, V. V. Konotop, and M. Salerno, Phys. Rev. A **64**, 043606 (2001).
[8] V. Ahufinger, A. Sanpera, P. Pedri, L. Santos, and M. Lewenstein, Phys. Rev. A **69**, 053604 (2004).
[9] V. V. Konotop and S. Takeno, Phys. Rev. B **55**, 11342 (1997).
[10] Y. Xiao and W. H. Hai, Phys. Lett. A **209**, 99 (1995).
[11] D. Hennig, Phys. Rev. E **59**, 1637 (1999).
[12] M. Kollmann, H. W. Capel, and T. Bountis, Phys. Rev. E **60**, 1195 (1999).
[13] M. J. Ablowitz, Y. Ohta, and A. D. Trubatch, Chaos, Solitons Fractals **11**, 159 (2000).
[14] C. S. Gardner, J. M. Greene, M. D. Kruskal, and R. M. Miura, Phys. Rev. Lett. **19**, 1095 (1967).
[15] V. E. Zhakharov and A. B. Shabat, Sov. Phys. JETP **34**, 62 (1972).
[16] M. J. Ablowitz and J. F. Ladik, J. Math. Phys. **16**, 598 (1975).
[17] M. J. Ablowitz and J. F. Ladik, J. Math. Phys. **17**, 1011 (1976).
[18] D. Cai, A. R. Bishop, and N. Grønbech-Jensen, Phys. Rev. E **52**, R5784 (1995).
[19] S. Ahmad and R. Chowdhury, J. Phys. A **20**, 293 (1987).
[20] L. Friedland and A. G. Shagalov, Phys. Rev. E **71**, 036206 (2005).
[21] E. M. McMillan, Phys. Rev. **68**, 143 (1945).
[22] V. I. Veksler, J. Phys. (USSR) **9**, 153 (1945).
[23] D. Bohm and L. Foldy, Phys. Rev. **70**, 249 (1946).
[24] B. Meerson and L. Friedland, Phys. Rev. A **41**, 5233 (1990).
[25] B. Meerson and S. Yariv, Phys. Rev. A **44**, 3570 (1991).
[26] S. Yariv and L. Friedland, Phys. Rev. E **48**, 3072 (1993).
[27] W. K. Liu, B. Wu, and J. M. Yuan, Phys. Rev. Lett. **75**, 1292 (1995).
[28] R. Malhotra, Sci. Am. **281**, 56 (1999).
[29] L. Friedland, Phys. Rev. E **61**, 3732 (2000).
[30] J. Fajans and L. Friedland, Am. J. Phys. **69**, 10 (2001).
[31] M. Khasin and L. Friedland, Phys. Rev. E **68**, 066214 (2003).
[32] M. Deutsch, B. Meerson, and J. E. Golub, Phys. Fluids B **3**, 1773 (1991).
[33] I. Aranson, B. Meerson, and T. Tajima, Phys. Rev. A **45**, 7500 (1992).
[34] L. Friedland, Phys. Fluids B **4**, 3199 (1992).
[35] L. Friedland, Phys. Rev. Lett. **69**, 1749 (1992).
[36] L. Friedland, Phys. Rev. E **55**, 1929 (1997).
[37] L. Friedland, Phys. Plasmas **5**, 645 (1998).
[38] L. Friedland and A. G. Shagalov, Phys. Rev. Lett. **81**, 4357 (1998).
[39] J. Fajans, E. Gilson, and L. Friedland, Phys. Plasmas **6**, 4497 (1999).
[40] L. Friedland and A. G. Shagalov, Phys. Rev. Lett. **85**, 2941 (2000).
[41] S. Glebov and O. Kiselev, J. Nonlinear Math. Phys. **12**, 330 (2002).
[42] O. Kiselev, S. Glebov, and V. Lazarev, math-ph/0410041 (unpublished).
[43] L. Friedland and A. G. Shagalov, Phys. Rev. Lett. **90**, 074101 (2003).
[44] J. Gómez-Gardeñes, L. M. Floría, M. Peyrard, and A. R. Bishop, Chaos **14**, 1130 (2004).